Energy & Environmental Science

Accepted Manuscript

ROYAL SOCIETY OF CHEMISTRY

www.rsc.org/ees

Broader Context

Hydrogen energy is currently pursued as a potential energy source and electrochemical water splitting process has been proposed as a promising and clean means for large scale hydrogen production. Limited by the high cost and scarcity of noble metal catalysts, non-noble metal catalysts are being explored as possible alternatives, with a few successful cases to date, *e.g.* MoS_2. However, the synthesis of these reported catalysts typically involve sophisticated methodologies in order to achieve desired nanostructures. Herein, we report a non-noble metal catalyst for hydrogen evolution reaction (HER), molybdenum phosphide. Its synthesis can be realized via a facile two-step-sintering method. Our experimental results show that even in its bulk form, molybdenum phosphide exhibits high performance in both acidic and alkaline conditions. Furthermore, observed performance of the bulk MoP was also comparable to that of the aforementioned nanostructured based catalysts. Theoretical calculations reveal that phosphorization can potentially modify the properties of metal and different degrees of phosphorization leads to distinct activities and stabilities.

Table of Content entry

Phosphorization of molybdenum leads to a good non-noble metal catalyst for hydrogen evolution reaction in both acidic and alkaline condition.

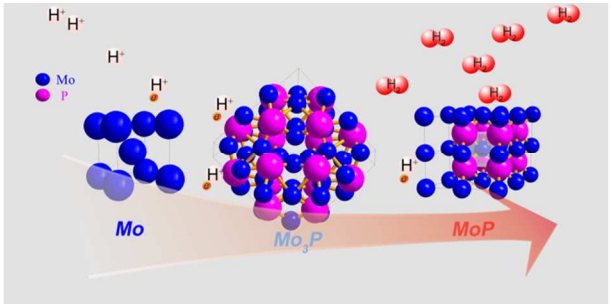

Molybdenum phosphide as an efficient electrocatalyst for hydrogen evolution reaction

Peng Xiao [a], Mahasin Alam Sk [a], Larissa Thia [c,d] , Xiaoming Ge [b], Rern Jern Lim [a], Jing-Yuan Wang [c], Kok Hwa Lim [a], Xin Wang [a]*

[a] School of Chemical and Biomedical Engineering, Nanyang Technological University, 50 Nanyang Avenue, 639798 Singapore

[b] Institute of Materials Research and Engineering (IMRE), Agency of Science, Technology, and Research (A*STAR), 3 Research Link, Singapore 117602, Singapore

[c] Residues and Resource Reclamation Centre, Nanyang Technological University

[d] Interdisciplinary Graduate School, Nanyang Technological University, 50 Nanyang Avenue Block S2 - B3a - 01, Singapore 639798, Singapore

* Corresponding author. E-mail: WangXin@ntu.edu.sg; Fax: +65 67947553

Abstract

Electrochemical production of hydrogen from water has been directed to the search of non-noble metal based and earth-abundant catalysts. In this work, we propose a novel cost-effective catalyst, molybdenum phosphide that exhibits high activity towards hydrogen evolution reaction (HER) in both acid and alkaline media even in bulk form. Comparative analysis of Mo, Mo_3P and MoP as catalysts for HER clearly indicates that phosphorization can potentially modify the properties of metal and different degrees of phosphorization lead to distinct activities and stabilities. Theoretical calculation by density functional theory also shows that a simple phosphorization of molybdenum to form MoP introduces a good 'H delivery' system which attains nearly zero binding to H at certain H coverage. With the combination of experimental facts and theoretical calculation, this work has enlightened a new way of exploring cost-effective catalysts for HER.

Key words

Hydrogen evolution reaction

Non-noble metal catalyst

Molybdenum phosphide

Density functional theory

Hydrogen chemisorption

Introduction

Hydrogen production through electrochemical water-splitting has been extensively pursued as it could potentially achieve a sustainable fuel production and the electricity required could be obtained from renewable energy [1]. Noble metals, *e.g.* Pt, demonstrate exceptional behavior with nearly zero overpotential in acidic media [2-4]. However, their high cost and scarcity impede their widespread usage and direct our attentions to earth-abundant metals or their compounds. Non-noble electrocatalysts can be categorized into two categories: (1) the derivatives of organic liganded metals (*e.g.* Ni, Mo, Fe), such as hydrogenases or metalloenzyme, the mimics of active site of hydrogenases [5, 6], molybdenum-oxo [5], pyrene-functionalized nickel complex [7]; (2) inorganic compounds of metals. MoS_2 [8-16], as a typical inorganic compound for hydrodesulfurization [17], was firstly discovered to possess biomimetic active sites as hydrogenases [18, 19]. Selenide [20, 21], nickel molybdenum nitride [22], carbide [23-26], nickel phosphide [27, 28], and first-row of transitional metal dichalcogenides [29] are reported to be promising electrocatalysts towards hydrogen evolution reaction (HER). By comparison, those cost-effective catalysts as the potential substitutes for Pt are either functionalized by organic ligand, *e.g.* [NiFe]hydrogenase or inorganics *e.g.* MoS_2, Ni_2P,. In a typical 'Volcano plot' of hydrogen adsorption energy of common metals (M = Nb, Mo, Ni, Pt, Au, Ag etc.) [30-32], it is revealed that strong metal-hydrogen (Mo, Ni etc.) bonds could impede hydrogen release from the active sites, compared to Pt group metals, *e.g.* Pd and Pt, which excludes those non-noble metals (*e.g.* Ni, Mo) as suitable candidates to catalyze hydrogen evolution reaction (HER). However, a subsequent study suggested that inorganic compounds of the non-noble metals can modify the metal-hydrogen bond strength and achieve a Pt-resembling Gibbs free energy for hydrogen evolution in acidic environment. The study of MoS_2 and Ni_2P has successfully underpinned this theoretical calculation[18, 33]. Inspired by this, herein, we report a molybdenum compound, MoP as a highly efficient catalyst for HER both in acidic and

alkaline media. Molybdenum phosphide is synthesized though facile sintering of molybdenum and phosphorus precursor assisted by citric acid. Unlike MoS_2 which shows very poor activity in bulk form, MoP still exhibits high electrocatalytic activity in bulk form. Furthermore, it was also experimentally demonstrated that going from metal Mo, Mo_3P to MoP, different degrees of phosphorization results in distinct performances and different stability. Theoretically, we employed Density functional theory (DFT) calculation to elucidate underlying reasons behind the distinct performance by comparing the hydrogen chemisorption process and Gibbs free energy between Mo, Mo_3P and MoP.

Results and Discussion

Mo_3P and MoP were synthesized at 800 °C and 650 °C respectively via a two-step sintering method (Experimental section, supporting information), whilst metal Mo was obtained by reducing MoO_3 in H_2 at 850 °C. Their corresponding XRD patterns are shown in Fig. 1. The peaks are well indexed to the standard XRD profiles and no major impurities are detected. Metal Mo, in a cubic pack (ICSD code: 643962) belongs to Im-3m (229). After incorporation phosphorus to form Mo_3P, it evolves to tetragonal structure. Its XRD pattern confirms its I-42m (121) in space group in Fig 1b, with Mo atom in either 2 or 4-coordinated by P atoms. Further phosphorization leads to MoP, in hexagonal structure (P-6m2), with Mo 6-coordinated by P atoms, as shown in Fig 1c. A more visualized structure change is presented in Scheme 1.

Field-emission scanning electron microscopy (FE-SEM) and Transmission electron microscopy (TEM) were applied to examine its morphology. FE-SEM graphs in Fig. 2a show that the as-synthesized MoP and Mo_3P (Figure S3) are in bulk form due to the calcination at high temperature. High-resolution TEM (HR-TEM) graph exhibits a well-arrayed (001) plane of MoP with the plane distance of 0.32 nm (Fig. 2b), which is correlated with the peak at 28° by XRD characterization. Energy dispersive X-ray spectroscopy (EDS) results confirm the compositions of MoP and Mo_3P (Figure S4), which is quite consistent with the chemical formulas, 1:1 and 3:1 for MoP, Mo_3P respectively. To elucidate the valence states of individual elements of MoP, X-ray photoelectron spectroscopy (XPS) experiments were conducted. Fig. 3a and 3b show the XPS profile of Mo 3d and P 2p of the as-synthesized MoP. Deconvolution of the spectra indicates two doublets at 235.28 eV/232.08 eV (Mo^{+6} $3d_{3/2}/3d_{5/2}$) and 231.9 eV/228.8 eV (Mo^{+4} $3d_{3/2}/3d_{5/2}$) in Fig. 3a, which can be assigned to high oxidation state of Mo (MoO_3 and MoO_2) [34, 35]. We believe that the oxidation only happens on the surface. To validate our hypothesis, we characterize the aged MoP (Figure S5)

by XRD, which still manifests the well-crystallized MoP and does not indicate any discernible peaks of the oxides, implying a mere surface-oxidation (less than 10 nm) that could only be detected by XPS. The rest of the XPS profile depicted in green (Fig. 3a) is ascribed to MoP, represented by a 231.2 eV/228.0 eV doublet, which agrees well with previous report [36, 37]. The profile of P 2p also exhibits a peak with high binding energy (peak 1 in Fig. 3b) which could be attributed to PO_4^{3-} or P_2O_5 [36] caused by oxidation. To identify the rest peaks for MoP, we further compared the XPS profile of the as-prepared MoP sample after test with the aged sample. As shown in Fig. 3d, P 2p profile of the aged sample does not display the low-binding-energy peaks as we can observe in Fig. 3b. On the contrary, it manifests even stronger peaks in the low-binding-energy region for the sample after test (Figure S6). Considering the above, we assign the doublet (130.1/129.2 eV for peak 2/peak 3) to low valence of P, MoP in this case.

In a three-electrode configuration, the catalytic activity towards HER was investigated in acid and alkaline media. Fig. 4 shows the performance of Mo, Mo_3P and MoP in acidic medium; Pt/C was also tested as a comparison. Polarization curve and Tafel slope ~ 30 mV dec^{-1} of Pt/C presented in Fig. 4a and 4b show consistency with previous studies [38]. Drop-casted on glassy carbon electrode (which exhibits negligible activity towards HER), to achieve the current density of 10 mA cm^{-2}, metal Mo requires the potential up to 0.5 V *vs.* RHE with the onset potential ~ 0.3 V *vs.* RHE, and Mo_3P is found to perform similarly as shown by the green line, indicating that metal Mo itself is not a good catalyst for HER and its phosphide Mo_3P is not suitable for HER either. In contrast, MoP shows a rather high performance in 0.5 M H_2SO_4. The onset of hydrogen evolution reaction can be observed at around 50 mV *vs.* RHE and the current density reaches 30 mA cm^{-2} at the potential of 0.18 V *vs.* RHE. To clarify these differences in performance, in the perspective of elementary step, *i.e.* hydrogen chemisorption, we use Gibbs free energy ($\Delta G°_H$) as the descriptor to assess the binding

strength of catalysts to H (*e.g.* Mo and MoP) and evaluate the catalysts (detailed DFT calculation can be found in supporting information). Metal Mo exhibits a strong binding to H, indicated by highly negative binding energy (ΔE_H) in Table S1 when H coverage reaches 1/4 monolayer (ML, one hydrogen adsorbed on 2×2 slab). This agrees well with previous report [18]. Calculation of Mo terminated surface on (001)-MoP also shows a similar or even stronger binding to H which excludes Mo as the active site. Nevertheless, the investigation of P sites implies that P has played a crucial role by acting as a 'hydrogen deliverer'. As shown in the Table S2, $\Delta G°_H$ changes from -0.36 eV to 0.54 eV when H coverage increases from 1/4 ML to full coverage, indicating that P could bond hydrogen at low coverage whilst desorb H at high coverage. This enables P to behave like a 'hydrogen deliverer', resembling the S-edges in MoS_2 [39]. Interestingly, when we applied the same method to calculate the binding energy of H on (001) of Mo_3P, where a four-P-site slab is chosen, the binding energy ΔE_H becomes positive (Table S3) with the initial two H adsorbed, indicating unfavorable binding of H on P site of Mo_3P. This is in accordance with experimental results.

After electrochemical testing, the catalyst composition was again examined by XPS. Compared to the as-synthesized MoP, XPS profile of the post-testing catalysts displays a similar profile to Mo 3d and P 2p shown in Figure S6 except for the decreased content of MoO_3 and MoO_2. Previous study of Mo_2C by Hu et al. [23] has proved that MoO_3 and MoO_2 are not efficient catalysts, which further suggests the high performance could be attributed to MoP.

Tafel plots of Potential *V*- Log|*j*(current density)| could be interpreted by Volmer-Tafel or Heyrovsky mechanism in the classical two-electron-reaction model for cathodic HER [24]. The Tafel slope of 92 mV dec^{-1} (Fig. 4b) for metal Mo suggests a typical Volmer-Tafel route with Volmer step as the rate-determining step. After phosphorization, it exhibits 147 mV dec^{-1} and 54 mV dec^{-1} for Mo_3P and MoP respectively. Here, the Tafel slope of 54 mV dec^{-1} implies

that hydrogen evolution on MoP undergoes a Heyrovsky mechanism which is still different from the route those noble metals, *e.g.* Pt, are subjected to. Based on the Langmuir Isotherm model [40], a fast discharging reaction (Volmer reaction) rate under low coverage (< 0.1) of adsorbed hydrogen (H_{ad}) leads to ~ 30 mV dec^{-1} and the Tafel slope of 54 mV dec^{-1} is most possibly caused by large coverage of H_{ad} (> 0.6). The large coverage of H is also rendered by theoretical calculation that zero $\Delta G°_H$ could be achieved at a certain coverage of H on P site from 2/4 ML to 3/4 ML. In comparison with metal Mo, we can conclude that a simple phosphorization could completely change the reaction route. By extrapolating the Tafel plot to overpotential of 0 V, the exchange current density can be extracted (Table 1). It is found that MoP exhibits a value of 3.4 $\times 10^{-2}$ mA cm^{-2}, ~ 70 times higher than that of metal Mo (4.9 $\times 10^{-4}$ mA cm^{-2}) and also outperforms MoS_2 that has been reported as a promising catalyst for HER [13, 20]. As a non-noble catalyst in bulk form, MoP has achieved comparably competitive performance as Ni_2P [27], and is even superior to MoB, Mo_2C [23], Mo_2C/CNT [25] at a similar loading for HER in acidic medium.

Few catalysts can exhibit good activity and stability under both acidic and alkaline conditions. *e.g.* Ni_2P was found to deteriorate rapidly in alkaline medium [27]. Herein we further examined the activity of MoP in both acidic and alkaline conditions using electrochemical impedance spectroscopy (EIS) technique. Bode plots of MoP (Figure S7) suggest a one-time-constant process in both acidic and alkaline media and Nyquist plots show a depressed arc intercepted by x-axis in Fig. 4c and 4d. The high-frequency intersection with x-axis represents ohmic resistance, mainly arising from the electrolyte and all contact resistances. To decouple the ohmic resistance from polarization resistance, we applied a model of an ohmic resistance (R_s) in series with a module, where a polarization resistance (R_{ct}) is in parallel with a constant phase element (CPE). As summarized in Table S4, MoP performs slightly better in alkaline medium than in acidic medium, indicated by smaller R_{ct} at the overpotential of 50 mV and

100 mV. Polarization curve in Fig. 5a agrees with the EIS results. At low current density, MoP in alkaline medium outperforms that in acidic medium, and exhibits nearly overlapped polarization curve at high-current region, suggesting a good performance in alkaline medium. Durability is a key factor in evaluating catalyst performance. Long-term stability is investigated both in 1 M KOH and 0.5 M H_2SO_4. Unfortunately, slow corrosion happens in 1M KOH as shown in an amperometric plot (Fig 5b) and the performance degrades to ca. 60% of its initial value in 40 h (Fig. 5a). However, chronoamperometric electrolysis evidences excellent stability of MoP in 0.5 M H_2SO_4 at applied potential of 0.14 mV *vs.* RHE in Fig. 5b, and no performance degradation was observed after electrolysis for more than 40 h. Polarization curve after electrolysis shows slightly enhanced performance at the region of low current density, which could be ascribed to surface activation in cathodic polarization. In contrast, Mo and Mo_3P suffer from severe performance degradation under both acidic and alkaline media. Inspection of morphology after stability test shows no difference compared to the one before test (Figure S8) in a panoramic view.

Mo is widely known as a chemically unstable metal in acidic media, and with insufficient phosphorization, the degradation of current density was observed even in the second scan of polarization curve of Mo_3P (not shown), implying that the corrosion occurs. Stability is commonly correlated with its structure. As shown in Scheme 1, Mo atom is 6-coordinated by P atom in MoP in contrast to 2 or 4 P-atoms bonded in Mo_3P, which could probably be related to the stability in acidic or alkaline media, and suggest the significance of phosphorization.

Conclusions

Distinct performance was observed from traditional metal Mo phosphide compound. Our results show catalysts having a higher degree of phosphorization as in MoP results in better performance compared to lower degree of phosphorization or lack thereof as in Mo_3P and Mo respectively. Performance in this case is determined based on polarization, Tafel analysis in the low-current region, stability test by chronoamperometric electrolysis.

DFT calculation verified that the active site should be ascribed to P atoms, which achieves nearly zero Gibbs free energy. The results entitle P atom the role analogous to S atom in MoS_2, which is responsible to create numbers of edges for HER [19]. In summary, we have demonstrated that facile phosphorization can transform metal Mo, a poor catalyst, to MoP, an active and stable catalyst for HER. Similar to organic-ligand-functionalized metal, *e.g.* nickel complex [7], molybdenum-oxo [5], this strategy could be easily extended to other earth-abundant and inexpensive metals (*e.g.* Ni, Fe *etc.*).

Acknowledgement

Financial support from the academic research fund AcRF tier 1 (M4011020 RG8/12) Ministry of Education, Singapore and competitive research program (2009 NRF-CRP 001-032), National Research Foundation, Singapore. The support by the Singapore National Research Foundation under its Campus for Research Excellence And Technological Enterprise (CREATE) programme is also acknowledged.

References

1. J. A. Turner, *Science*, 2004, **305**, 972-974.
2. R. Cammack, *Nature*, 1999, **397**, 214-215.
3. A. Volbeda and J. C. Fontecilla-Camps, *Dalton Trans.*, 2003, 4030-4038.
4. S. Shima, O. Pilak, S. Vogt, M. Schick, M. S. Stagni, W. Meyer-Klaucke, E. Warkentin, R. K. Thauer and U. Ermler, *Science*, 2008, **321**, 572-575.
5. H. I. Karunadasa, C. J. Chang and J. R. Long, *Nature*, 2010, **464**, 1329-1333.
6. A. Le Goff, V. Artero, B. Jousselme, P. D. Tran, N. Guillet, R. Métayé, A. Fihri, S. Palacin and M. Fontecave, *Science*, 2009, **326**, 1384-1387.
7. P. D. Tran, A. Le Goff, J. Heidkamp, B. Jousselme, N. Guillet, S. Palacin, H. Dau, M. Fontecave and V. Artero, *Angew. Chem. Int. Ed.*, 2011, **50**, 1371-1374.
8. D. Merki and X. Hu, *Energy Environ. Sci.*, 2011, **4**, 3878-3888.
9. I. Hatay, P. Y. Ge, H. Vrubel, X. Hu and H. H. Girault, *Energy Environ. Sci.*, 2011, **4**, 4246-4251.
10. H. Vrubel, D. Merki and X. Hu, *Energy Environ. Sci.*, 2012, **5**, 6136-6144.
11. J. Xie, H. Zhang, S. Li, R. Wang, X. Sun, M. Zhou, J. Zhou, X. W. Lou and Y. Xie, *Adv. Mater.*, 2013, **25**, 5807-5813.
12. Z. Chen, D. Cummins, B. N. Reinecke, E. Clark, M. K. Sunkara and T. F. Jaramillo, *Nano Lett.*, 2011, **11**, 4168-4175.
13. J. Kibsgaard, Z. Chen, B. N. Reinecke and T. F. Jaramillo, *Nat. Mater.*, 2012, **11**, 963-969.
14. M. A. Lukowski, A. S. Daniel, F. Meng, A. Forticaux, L. Li and S. Jin, *J. Am. Chem. Soc.*, 2013, **135**, 10274-10277.
15. D. Merki, S. Fierro, H. Vrubel and X. Hu, *Chem. Sci.*, 2011, **2**, 1262-1267.
16. J. D. Benck, Z. Chen, L. Y. Kuritzky, A. J. Forman and T. F. Jaramillo, *ACS Catal.*, 2012, **2**, 1916-1923.
17. R. R. Chianelli, M. H. Siadati, M. P. De la Rosa, G. Berhault, J. P. Wilcoxon, R. Bearden and B. L. Abrams, *Cat. Rev.: Sci. Eng.*, 2006, **48**, 1-41.
18. B. Hinnemann, P. G. Moses, J. Bonde, K. P. Jørgensen, J. H. Nielsen, S. Horch, I. Chorkendorff and J. K. Nørskov, *J. Am. Chem. Soc.*, 2005, **127**, 5308-5309.
19. T. F. Jaramillo, K. P. Jørgensen, J. Bonde, J. H. Nielsen, S. Horch and I. Chorkendorff, *Science*, 2007, **317**, 100-102.
20. D. Kong, H. Wang, J. J. Cha, M. Pasta, K. J. Koski, J. Yao and Y. Cui, *Nano Lett.*, 2013, **13**, 1341-1347.
21. H. Wang, D. Kong, P. Johanes, J. J. Cha, G. Zheng, K. Yan, N. Liu and Y. Cui, *Nano Lett.*, 2013, **13**, 3426-3433.
22. W.-F. Chen, K. Sasaki, C. Ma, A. I. Frenkel, N. Marinkovic, J. T. Muckerman, Y. Zhu and R. R. Adzic, *Angew. Chem. Int. Ed.*, 2012, **51**, 6131-6135.
23. H. Vrubel and X. Hu, *Angew. Chem. Int. Ed.*, 2012, **51**, 12703-12706.
24. W.-F. Chen, S. Iyer, S. Iyer, K. Sasaki, C.-H. Wang, Y. Zhu, J. T. Muckerman and E. Fujita, *Energy Environ. Sci.*, 2013, **6**, 1818-1826.
25. W.-f. Chen, C. H. Wang, K. Sasaki, N. Marinkovic, W. Xu, J. T. Muckerman, Y. Zhu and R. R. Adzic, *Energy Environ. Sci.*, 2013, **6**, 943-951.
26. L. Liao, S. Wang, J. Xiao, X. Bian, Y. Zhang, M. D. Scanlon, X. Hu, Y. Tang, B. Liu and H. H. Girault, *Energy Environ. Sci.*, 2014, **7**, 387-392.
27. E. J. Popczun, J. R. McKone, C. G. Read, A. J. Biacchi, A. M. Wiltrout, N. S. Lewis and R. E. Schaak, *J. Am. Chem. Soc.*, 2013, **135**, 9267-9270.
28. L. Feng, H. Vrubel, M. Bensimon and X. Hu, *Phys. Chem. Chem. Phys.*, 2014, **16**, 5917-5921.

29. D. Kong, J. J. Cha, H. Wang, H. R. Lee and Y. Cui, *Energy Environ. Sci.*, 2013, **6**, 3553-3558.
30. J. K. Nørskov, T. Bligaard, A. Logadottir, J. R. Kitchin, J. G. Chen, S. Pandelov and U. Stimming, *J. Electrochem. Soc.*, 2005, **152**, J23-J26.
31. W. Schmickler and S. Trasatti, *J. Electrochem. Soc.*, 2006, **153**, L31-L32.
32. J. K. Nørskov, T. Bligaard, A. Logadottir, J. R. Kitchin, J. G. Chen, S. Pandelov and U. Stimming, *J. Electrochem. Soc.*, 2006, **153**, L33.
33. P. Liu and J. A. Rodriguez, *J. Am. Chem. Soc.*, 2005, **127**, 14871-14878.
34. X. Zhao, M. Cao, B. Liu, Y. Tian and C. Hu, *J. Mater. Chem.*, 2012, **22**, 13334-13340.
35. O. G. Marin Flores and S. Ha, *Appl. Catal. A Gen.*, 2009, **352**, 124-132.
36. J. Bai, X. Li, A. Wang, R. Prins and Y. Wang, *J. Catal.*, 2012, **287**, 161-169.
37. D. C. Phillips, S. J. Sawhill, R. Self and M. E. Bussell, *J. Catal.*, 2002, **207**, 266-273.
38. Y. Li, H. Wang, L. Xie, Y. Liang, G. Hong and H. Dai, *J. Am. Chem. Soc.*, 2011, **133**, 7296-7299.
39. A. B. Laursen, S. Kegnaes, S. Dahl and I. Chorkendorff, *Energy Environ. Sci.*, 2012, **5**, 5577-5591.
40. J. G. N. Thomas, *Trans. Faraday Soc.*, 1961, **57**, 1603-1611.

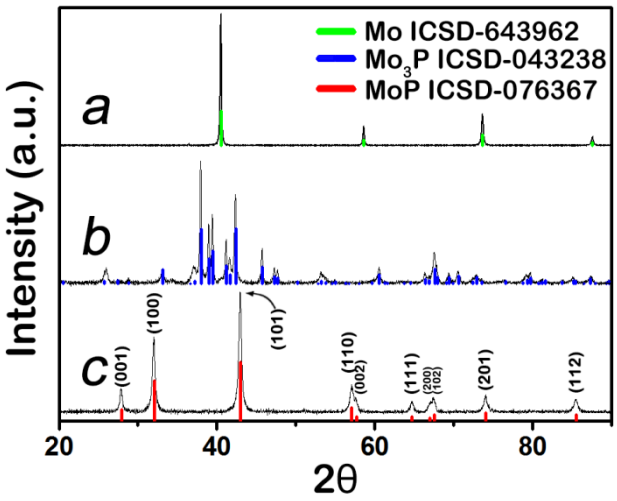

Fig. 1 XRD patterns of (a) Mo; (b) Mo_3P; (c) MoP.

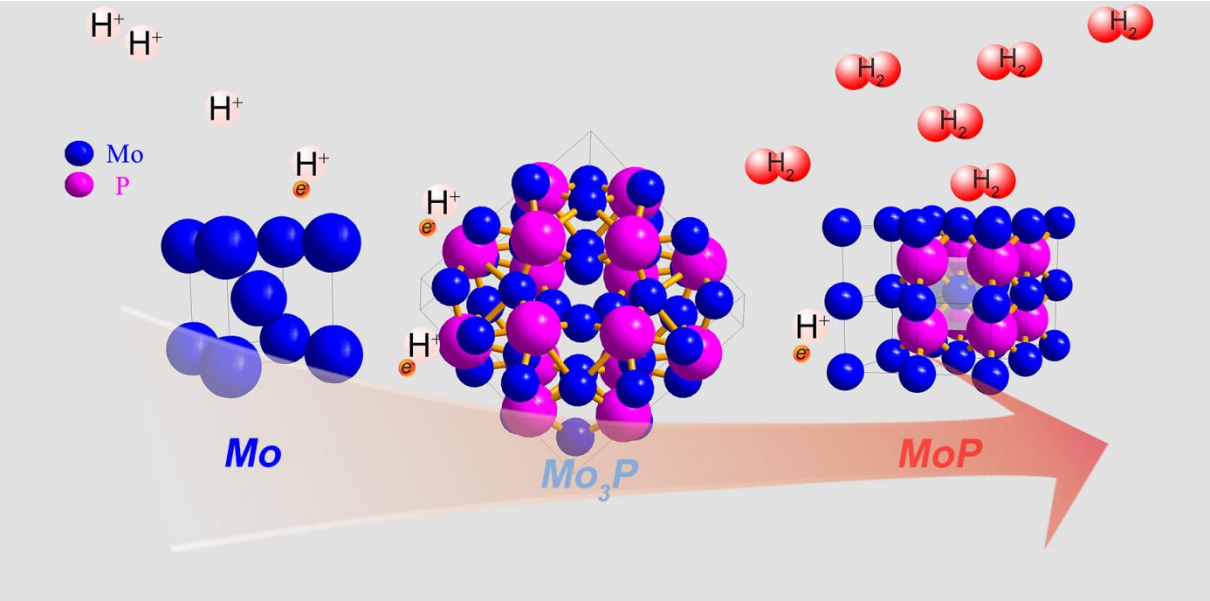

Scheme 1 schematic graph to show the structural evolution upon phosphorization

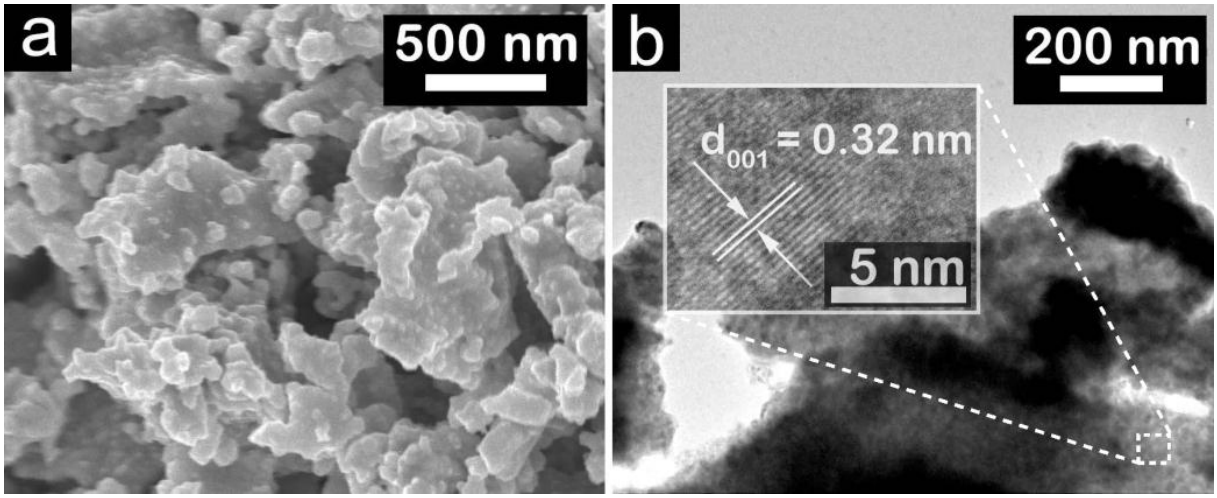

Fig. 2 Morphology of MoP (a) FE-SEM and (b) TEM graph.

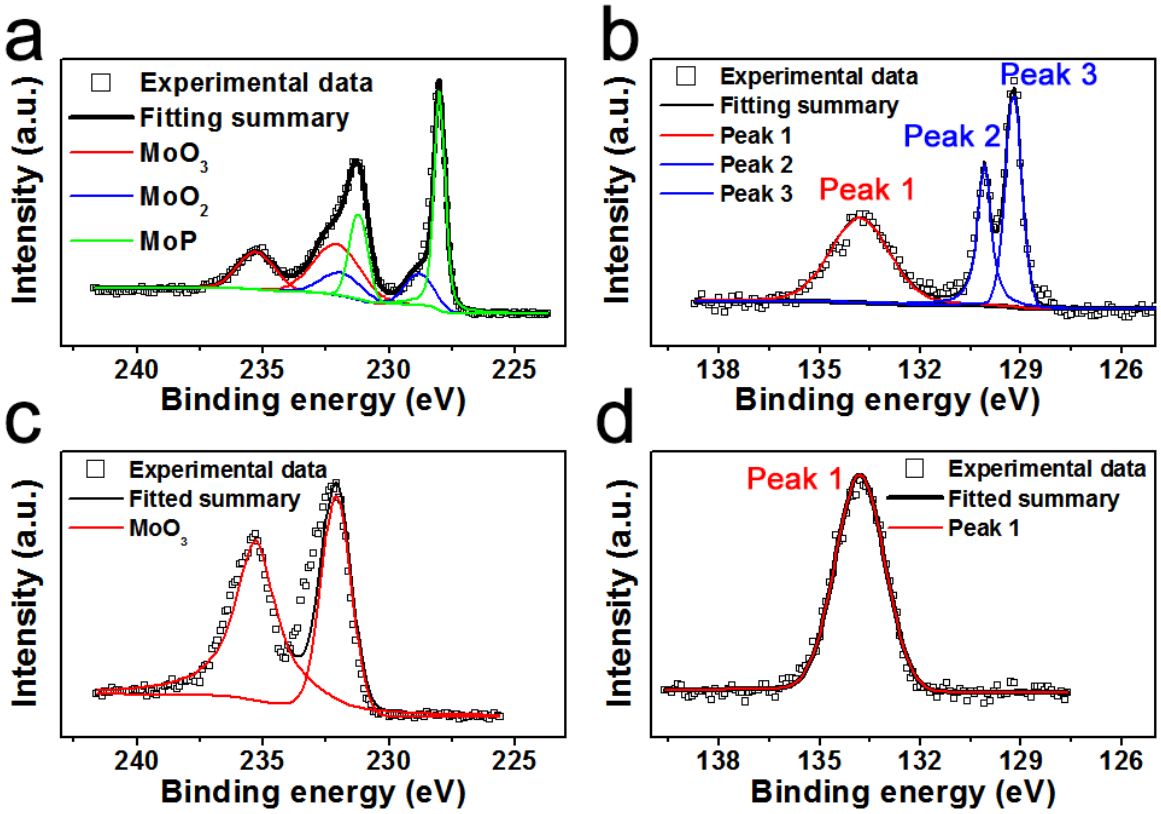

Fig. 3 X-ray photoelectron spectra (XPS) of the as-synthesized MoP (a) Mo 3d and (b) P 2p; aged MoP (c) Mo 3d and (d) P 2p.

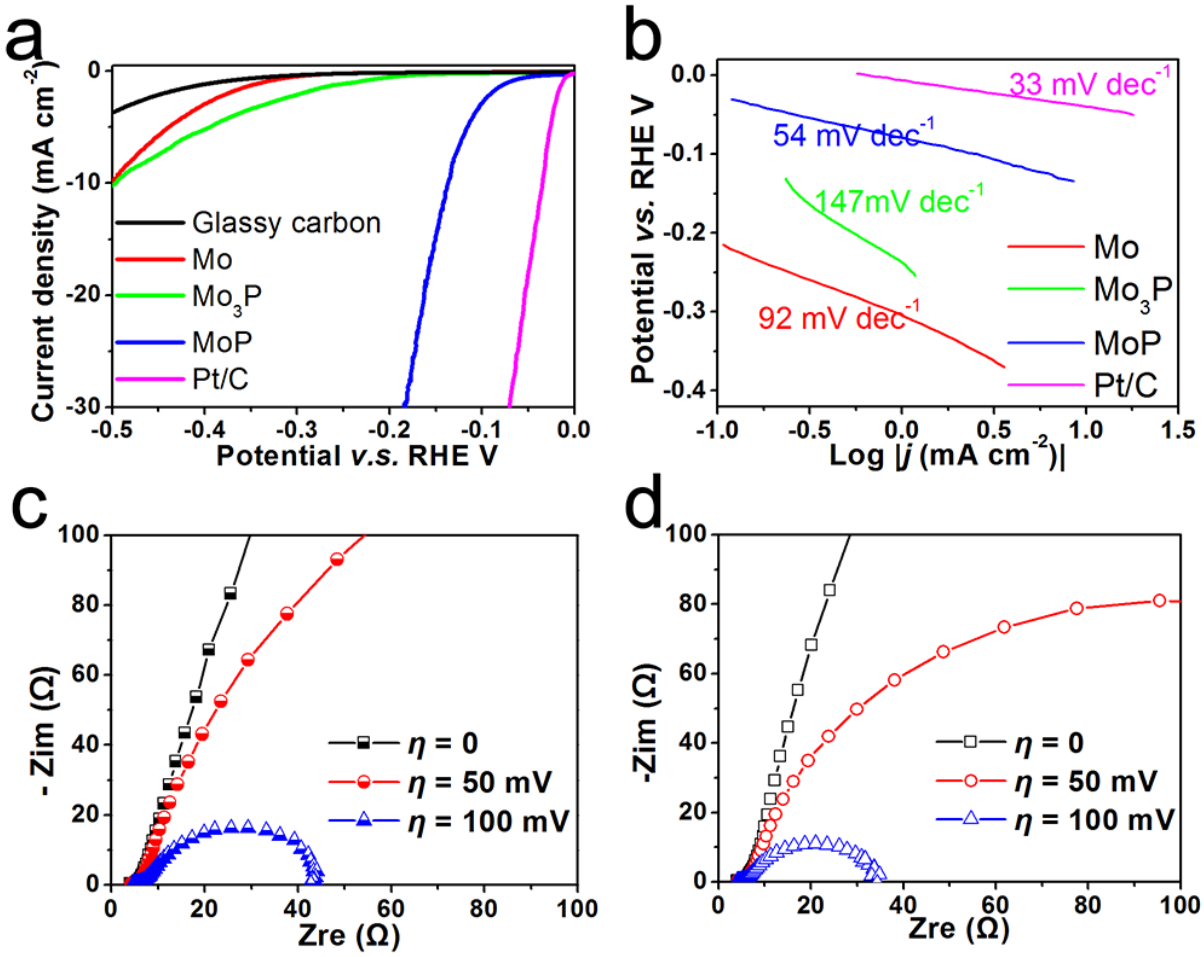

Fig. 4 (a) Polarization curves of Mo, Mo_3P and MoP in 0.5 M H_2SO_4, scan rate: 2 mV s^{-1}; (b) Tafel plots in 0.5 M H_2SO_4; Electrochemical impedance spectra of MoP: (c) in 0.5 M H_2SO_4 and (d) in 1 M KOH.

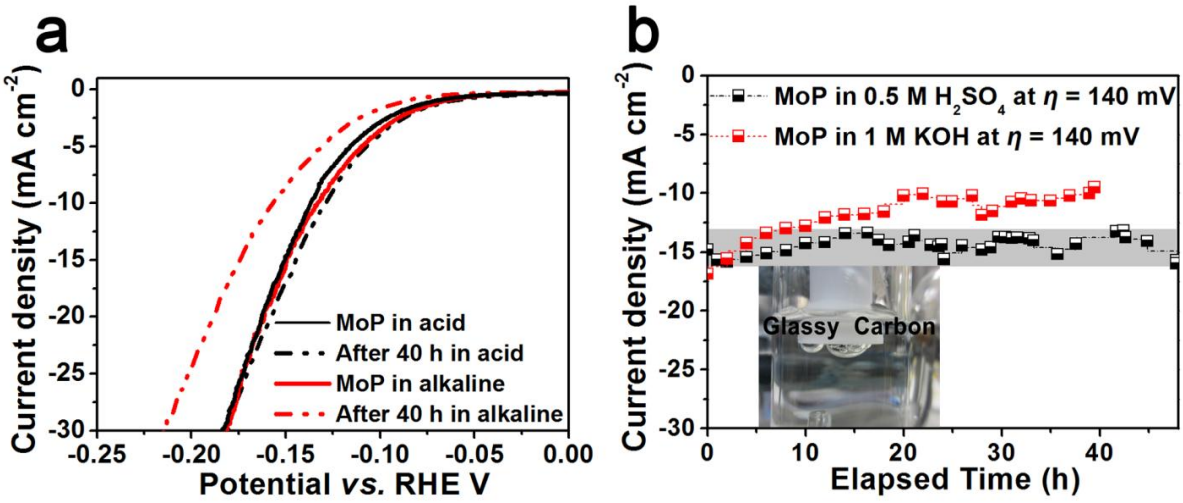

Fig. 5 (a) polarization curve before and after durability test, scan rate: 2 mV s^{-1}; (b) chronoamperometric electrolysis;

Table 1 Tafel slope ***b*** and exchange current density j_o

	b **(mV dec^{-1})**	j_o **(mA cm^{-2})**
Mo	92	4.9×10^{-4}
Mo_3P	147	--
MoP in 0.5 M H_2SO_4	54	3.4×10^{-2}
MoP in 1 M KOH	48	4.6×10^{-2}
Pt/C	33	0.63